Nuclear Science and Techniques (2025) 36:179
https://doi.org/10.1007/s41365-025-01756-7

Lifetime of first excited state in ^{139}La and the role of core-excitation on L-forbidden M1 transition

Zhi-Xuan Wang[1] · Guang-Xin Zhang[1] · Wei Jiang[2] · Meng-Lan Liu[1] · Cen-Xi Yuan[1] · Bo-Shuai Cai[1] · Chong Qi[3] · Hong-Yi Wu[4,5] · Zhi-Huan Li[5] · Yong-Hao Chen[2] · Rui-Rui Fan[2] · Kang Sun[2] · Wei Wang[1] · Jun Su[1] · Long Zhu[1] · Yue-Huan Wei[1] · Yu-Mei Zhang[1] · Wei Hua[1] · Bo Mei[1] · Xiao Fang[1] · Yi-Nu Zhang[1] · Chen-Chen Guo[1] · Sheng-Li Chen[1] · Xiao-Peng Zhou[6]

Received: 6 July 2024 / Revised: 26 December 2024 / Accepted: 15 January 2025 / Published online: 17 July 2025

Abstract

This study determined the lifetime of the first excited state ($5/2^+_1$) in ^{139}La via β–γ time-difference measurement using a $LaBr_3$ + plastic scintillator array. This state is populated following the decay of ^{139}Ba produced in the ^{138}Ba(n,γ) reaction. Compared with previous experiments using only stilbene/plastic crystals, this experiment separates the background contribution in the γ-ray spectrum owing to the high energy resolution of $LaBr_3$. The L-forbidden M1 transition strength, B(M1, $5/2^+_1 \rightarrow 7/2^+_1$), in ^{139}La was measured and compared with detailed large-scale shell model calculations, with a special focus on the core-excitation effect. The results showed the importance of both proton and neutron core-excitations in explaining the M1 transition strength. Meanwhile, the effective g-factor for the tensor term of the M1 operator was smaller than the previously reported value in this region or around ^{208}Pb.

Keywords L-forbidden M1 transition · Effective g-factor · $LaBr_3$ · Fast-timing measurement

1 Introduction

L-forbidden M1 transitions have been reported in many odd-mass nuclei, involving pairs of low-lying excited and ground states of single particle nature with the orbital angular momenta differing by two units, such as $g_{7/2}$-$d_{5/2}$, $s_{1/2}$-$d_{3/2}$, and $p_{3/2}$-$f_{5/2}$ [1]. The corresponding orbitals are typically close to each other outside the shell closure. In principle, the M1 transition between them is forbidden. The observation of these nonzero transition strengths indicates the M1 transition of L-forbidden nature beyond a single-particle scheme.

This work was supported by the Guangdong Major Project of Basic and Applied Basic Research (No. 2021B0301030006), Young Scientists Fund of the National Natural Science Foundation of China (No. 12405144), the National Natural Science Foundation of China (No. 12475129), the International Atomic Energy Agency Coordinatated Research Project F41034 (No. 28649), the computational resources from Sun Yat-sen University the National Supercomputer Center in Guangzhou, and the Natural Science Foundation of Guangdong Province, China (No. 2025A1515012112).

✉ Guang-Xin Zhang
zhanggx37@mail.sysu.edu.cn

Cen-Xi Yuan
yuancx@mail.sysu.edu.cn

[1] Sino-French Institute of Nuclear Engineering and Technology, Sun Yat-Sen University, Zhuhai 519082, China

[2] Spallation Neutron Source Science Center, Dongguan 523803, China

[3] KTH Royal Institute of Technology, 10691 Stockholm, Sweden

[4] Key Laboratory of Nuclear Data, China Institute of Atomic Energy, Beijing 102413, China

[5] School of Physics and State Key Laboratory of Nuclear Physics and Technology, Peking University, Beijing 100871, China

[6] School of Physics, Beihang University, Beijing 100191, China

The effective g-factor is necessary to explain the observed magnetic momentum or M1 transition strength. From a physics perspective, such effective operators originate from core polarization and the meson exchange effect [2, 3]. Compared with the spin and orbital terms, the tensor term of the effective M1 operator is almost negligible when a magnetic momentum is produced, as mentioned in Refs. [2–4]. However, in the L-forbidden M1 transition, the tensor term ($[Y_2, s]$) is essential because it connects the orbitals with $\Delta l = 2$.

Meanwhile, the core-excitation, especially when crossing $Z = 50$ or $N = 50$ shells [5, 6], increases the number of single-particle orbitals contributing to the M1 transition. However, the quantitative influence of the core polarization effect on the effective g-factor has not yet been elucidated, particularly the tensor term. The L-forbidden M1 transitions in odd-mass isotopes along the $N = 82$ isotonic chain are potential tools for investigating an effective M1 operator.

The adopted lifetime of the first excited state in ^{139}La [7] was determined in previous experiments conducted using the β decay channel from either ^{139}La or ^{139}Ce. However, because of material limitation, most experiments use two stilbene scintillators to measure the time differences between β-rays and conversion electrons, yielding a half-life of 1.50(10) ns in both cases, Refs. [8, 9]. An alternative method is using stilbene and plastic crystals to measure the time difference between conversion electrons and KX-rays, as mentioned in Refs. [10, 11], yielding half-lives of 1.47(6) ns and 1.60(4) ns, respectively. Although the aforementioned experiments employed the best available instruments, the lack (or insufficiency) of energy-resolving power limited the operations of the detectors, accounting for possible uncertainties in the background subtraction. Currently, $LaBr_3$ detectors are widely used for γ-ray spectroscopy [12–15]. Owing to its excellent time and energy resolution, the $LaBr_3$ detector together with plastic scintillators is a potential tool for determining the lifetime of the first excited state in ^{139}La via β–γ time-difference measurement, an operation that was previously impossible. This novel measurement technique could eliminate the γ-ray background and be applied to investigate complex β-decay channels. Moreover, it could analyze radioactive isotopes such as ^{133}Sn, ^{135}Te, and ^{137}Xe or determine the lifetime of the first excited states in ^{133}Sb, ^{135}I, and ^{137}Cs via β–γ time-difference measurement.

This study experimentally performed β–γ measurement to determine the first excited state in ^{139}La using $LaBr_3$ and plastic scintillators. Based on the experimental results, a comprehensive shell-model study on the L-forbidden M1 transition was conducted, focusing on the effect of core-excitation. Experimental details and results are presented in Sect. 2, and the discussion is presented in Sect. 3.

2 Experimental setup and result

The experiment was conducted using the Back-n white neutron beamline [16–21] located at the China Spallation Neutron Source (CSNS) [22]. The Back-n beamline uses backstreaming white neutrons from the spallation target at CSNS, delivering an intense flux of over $\sim 10^7 \mathrm{cm}^{-2}\mathrm{s}^{-1}$ at the experimental hall I, which is 55 m away from the spallation target. With a proton beam power of 100 kW, the Back-n neutron energy ranges from 0.3 eV to several hundreds of megaelectron volts. Three natural Ba targets (71.689% of ^{138}Ba) with diameters of 30 mm were placed on the beamline; one target was 3-mm thick, and the others were 5 mm-thick.

During irradiation, ^{139}Ba was mainly produced in the ^{138}Ba(n,γ) reaction. Given that the β-decay half-life of ^{139}Ba is 82.93(9) minutes [7], the irradiation time on the beamline was approximately 4 h. After irradiation, the beam was stopped and the targets were displaced to another location for off-beam decay measurement, which lasted 4 h; after which, all the samples were irradiated for 4 h. The procedure was repeated several times. In this experiment, both the irradiation and measurement times were 20 h.

As shown in Fig. 1, for off-line measurement, one plastic scintillator and two $LaBr_3$ detectors were installed on the samples to detect β and γ rays, respectively. A 2-mm-thick EJ-200 plastic scintillator of size 3 cm × 4 cm, coupled with XP2020 photomultiplier tubes (PMTs), was used. The crystal of each $LaBr_3$ has a diameter of 2 in

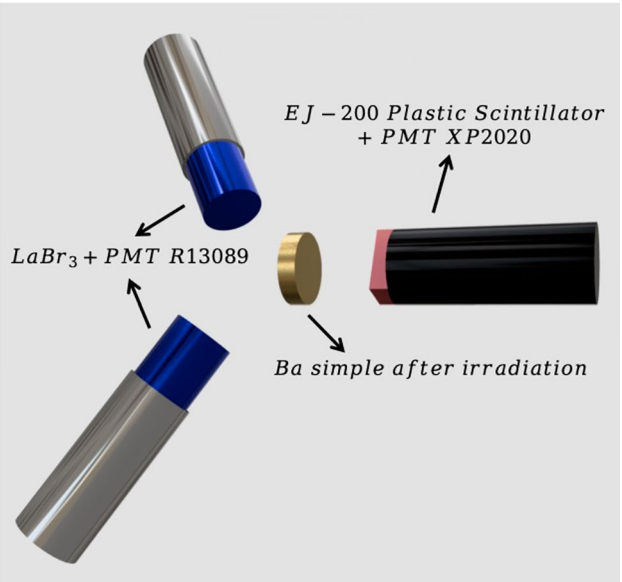

Fig. 1 (Color online) Experimental setup, including two $LaBr_3$ detectors and one plastic scintillator coupled with a XP2020 photomultiplier tube

(50.8 mm) and length of 3 in (76.2 mm). The signal from each $LaBr_3$ crystal was captured using Hamamatsu PMT R13089, whose anode output has a typical rise time of 2 ns, suitable for fast-timing measurement. The signals from all three detectors were transmitted to a Pixie-16 module from XIA LLC, which is a 14-bit 500 MHz Digital Pulse Processor [23]. To improve the time resolution, a CFD algorithm was applied to detect the zero-crossing of a pulse by subtracting the scaled and delayed copies of the fast-filter pulse in the general-purpose digital data acquisition system (GDDAQ) developed by Peking University. Detailed information on GDDAQ and related CFD logic can be obtained in Ref. [23],

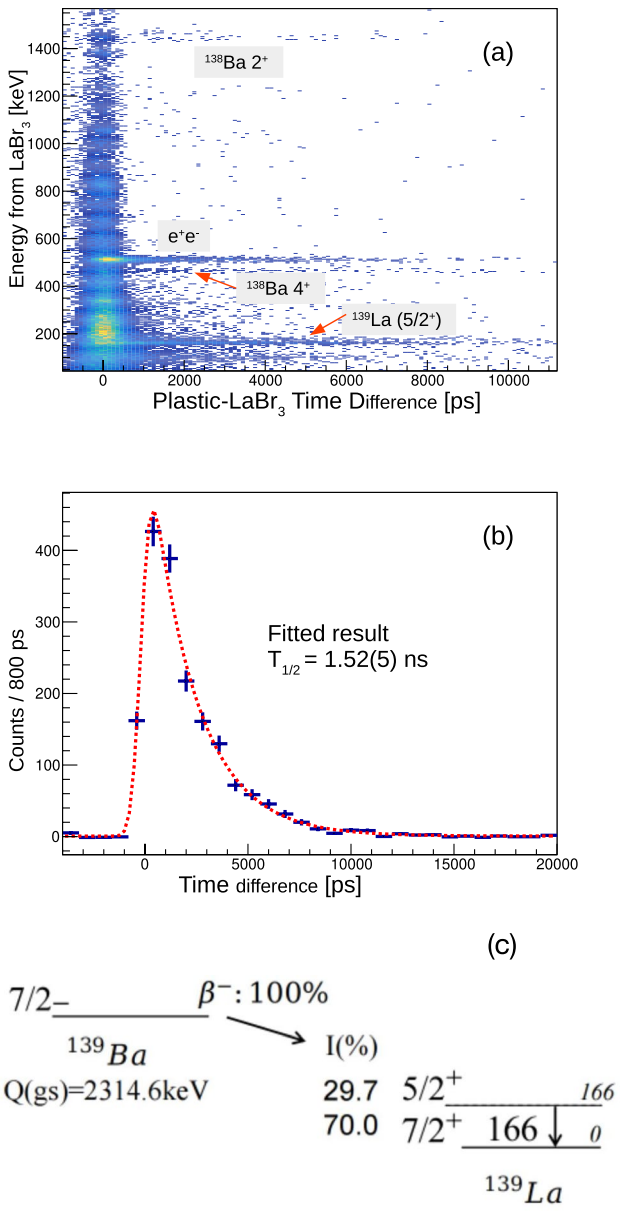

Fig. 2 (Color online) **a** γ Energy versus β–γ time-difference plot, in which the β decays to excited states in ^{138}Ba and ^{139}La are separated. **b** β–γ time-difference distribution and fitted result of the half-life of first excited state in ^{139}La. **c** Partial β decay scheme illustrating the dominant decay channel from ^{139}Ba to the first excited state in ^{139}La

Figure 2a shows a two-dimension plot of the β–γ time difference vs γ-ray energy. Following the β decay, three γ lines at 166, 462, and 1436 keV were observed in addition to the 511 keV transition, corresponding to the decay of the first excited state in ^{139}La [7] and 2_1^+ and 4_1^+ states in ^{138}Ba [24], respectively. These results are consistent with the observation that all the aforementioned transitions attain the highest intensities in their respective β-decay channels [7, 24], whereas the other weak transitions cannot easily be observed, considering the statistics and energy resolution of $LaBr_3$ detectors.

When high-energy neutrons impinge on ^{138}Ba, ^{139}Ba is produced with an excitation energy higher than the proton separation energy (9316(9) keV [7]), producing ^{138}Cs using proton evaporation channels. The ground state of ^{138}Cs has a β-decay half-life of 32.5(5) min [24], and most of the β-decay branches feed on excited states higher than the 4_1^+ state in ^{138}Ba. Considering that the 4_1^+ state is an isomeric state with $T_{1/2} = 2.160(11)$ ns, transitions of 462 and 1436 keV may be observed in the β-delayed γ-ray spectrum, as shown in Fig. 2a.

The following paragraph focuses on the $^{139}\text{Ba} \rightarrow {}^{139}\text{La}$ β -decay channel. The β-decay channel has been extensively investigated [7–11]. The branching ratio information reveals that approximately 70% would directly populate the ground state in ^{139}La without emitting γ rays. The strongest among the remaining branches feeds the first excited state in ^{139}La with a ratio of 29.7%, and all the remaining branches only account for 0.3% of the decay strength. Consequently, most of the measured β–γ coincidence events are related to the ground state of ^{139}Ba β decay to the $5/2_1^+$ state in ^{139}La, followed by the $5/2_1^+ \rightarrow 7/2_1^+$ γ ray at 166 keV. By deconvolution fitting [14, 15] the β–γ time difference with a γ-ray energy of 166 keV, the lifetime of $5/2_1^+$ in ^{139}La is 1.52(5) ns, as shown in Fig. 2. This value is consistent with that adopted in the NNDC website [7].

The fitting function includes the contributions of both prompt response functions and the exponential decay component. Detailed information about the fitting can be obtained in Ref. [15] and references therein. In the current experiment, owing to the excellent energy resolution of $LaBr_3$, the 166-keV transition can easily be selected, facilitating background subtraction, as shown in Fig. 2, an operation that was impossible in the 1960 s.

3 Shell-model investigation and discussion

Shell model calculations have been performed to investigate the nature of the L-forbidden M1 transition in ^{139}La. To examine the effect of core-excitation, the model space comprises $\pi 0g_{9/2}$, $0g_{7/2}$, $1d_{5/2}$, $1d_{3/2}$, $2s_{1/2}$, $0h_{11/2}$ and $\nu 0h_{11/2}$, $0h_{9/2}$, $1f_{7/2}$, $1f_{5/2}$, $2p_{3/2}$, $2p_{1/2}$, $0i_{13/2}$ orbitals. The proton (neutron) core-excitation across the $Z = 50$ ($N = 82$) shell can be achieved by exciting protons (neutrons) from the $\pi 0g_{9/2}$ ($\nu 0h_{11/2}$) orbital to higher orbitals.

The effective Hamiltonian is based on the nuclear force V_{MU}+LS [26], which comprises a Gaussian central force, a $\pi + \rho$ meson-exchange tensor force, and an M3Y spin-orbit force [27]. The V_{MU}+LS force has been employed in the *psd* [28], *sdpf* [29], *pfsdg* regions [30], and nearby regions around ^{132}Sn [31, 32] and ^{208}Pb [4, 33–35]. Recently, V_{MU} +LS had been employed to investigate the level structure of nuclei around ^{132}Sn and ^{208}Pb [36, 37] in a unified manner. Specifically, the separation and excitation energies, as well as the nuclear level densities of $50 \le Z \le 56$ and $80 \le N \le 84$ nuclei, were reproduced using the interaction proposed in Ref. [38]. All the shell-model calculations were performed using the code KSHELL [39].

1. Influence of effective g-factor on lifetime prediction

In this study, $B(M1)$ calculation employed effective g-factors of $g_p^l = 1$, $g_n^l = 0$, $g_p^s = 5.0274$, and $g_n^s = -3.4424$. The former two are the free-nucleon values, and the latter two are obtained from the free g-factor quenched by 0.9. The proton and neutron effective charges are 1.5e and 0.5e in the $B(E2)$ calculation, respectively.

The theoretical predictions of the $5/2_1^+ \rightarrow 7/2_1^+$ transition strength in ^{139}La under different conditions are presented in Table 1. Eliminating core-excitation yields a $B(M1)$ value of 2.2×10^{-5} [μ_N^2], increasing the half-life to 97.5 ns, even when the E2 strength is considered. By exciting either one proton or neutron across their respective major shell (noted as "p1" or "n1" in Table 1), the predicted M1 strength becomes one order of magnitude higher. Thus, the predicted half-life is significantly consistent with the experimentally measured half-life, such as 9.5 and 21.5 ns for the proton and neutron cases, respectively. Because of the limitation of computer power, the maximum truncation in the current calculation is that one proton and one neutron can be excited from the ^{132}Sn core, noted as "p1n1" in the last column of Table 1. Here, the maximum $B(M1)$ is 1.3×10^{-3} [μ_N^2], which is approximately two orders of magnitude larger than that in the no core-excitation case. Notably, the influence of the core-excitation on the $B(E2)$ strength is significantly reduced. This study shows that a quenching factor of 0.9 is sufficient considering core-excitation with only a 1p-1h configuration. This value is significantly consistent with the free-nucleon value obtained via the meson exchange calculation (MEC) [40] in the limited model space around the ^{132}Sn region [41, 42].

The calculation in the previous paragraph did not include the tensor term in the effective g-factor [43, 44]. Meanwhile, the tensor part, exhibiting a slight influence on the magnetic moments around the ^{132}Sn region, as reported in Ref. [41, 42], is essential for the L-forbidden M1 transition strength because the $g_{\rm eff}^t[Y_2, s]$ operator can have a nonzero off-diagonal matrix element in the $d_{5/2} \rightarrow g_{7/2}$ transition. The last two columns in Table 1 present the shell-model calculation performed by using the effective M1 operator with the tensor part. With a slight correction, $g_p^t = 0.15$ (compared with a value greater than 3 obtained via MEC, as shown in Refs. [41, 42]) and $g_n^t = 0$, the calculation is consistent with the experimental result in the "p1n1" case, as presented in Table 1.

2. Detailed investigation on M1 matrix element

Furthermore, we analyzed the difference in the M1 matrix element, particularly for the high-J component, between different core-excitation conditions. The decomposition of the M1 matrix element is shown in Fig. 3. First, the inclusion of proton core-excitation significantly enhances the contribution from the $\pi g_{7/2}$ and $g_{9/2}$ shells.

Neutron core-excitation introduces a strong component from νh orbitals similarly. In the one-proton–one-neutron

Table 1 Theoretical predictions of the $5/2^+ \rightarrow 7/2^+$ transition strength in ^{139}La with different truncations

Core-excitation	$B(M1)$ [μ_N^2]	$T_{1/2}^{\rm partial}$(M1) [ns]	$B(E2)$ [e^{2}fm^4]	$T_{1/2}^{\rm partial}(E2)$ [ns]	$T_{1/2}^{\rm total}$ [ns]	$B(M1)^*$ [μ_N^2]	$T_{1/2}^{\rm total*}$ [ns]
None	2.2×10^{-5}	309.8	0.938	142.3	97.5	1.5×10^{-3}	4.5
p1	6.9×10^{-4}	9.9	0.478	279.5	9.5	3.5×10^{-3}	1.9
n1	2.8×10^{-4}	24.6	0.802	166.5	21.5	2.5×10^{-3}	2.7
p1n1	1.3×10^{-3}	5.4	0.348	383.9	5.3	4.6×10^{-3}	1.5

The absence of core-excitation indicates that no nucleon can be excited from the fully occupied $\pi 0g_{9/2}$ and $\nu h_{11/2}$ orbitals. p1 and n1 indicate that only one proton and one neutron can be prompted from the $\pi 0g_{9/2}$ and $\nu h_{11/2}$ orbitals, respectively. p1n1 indicates the condition that one proton and one neutron can cross their $Z = 50$ or $N = 82$ major shell. The inner conversion coefficients of the M1 and E2 components for the measured 166-keV transition are 0.26 and 0.34 by BRICC [25], respectively. The $B(M1)^*$ and $T_{1/2}^{\rm total*}$ represent the condition in which the effective M1 operator considers the tensor part with $g_t = 0.15$ and 0 for proton and neutron

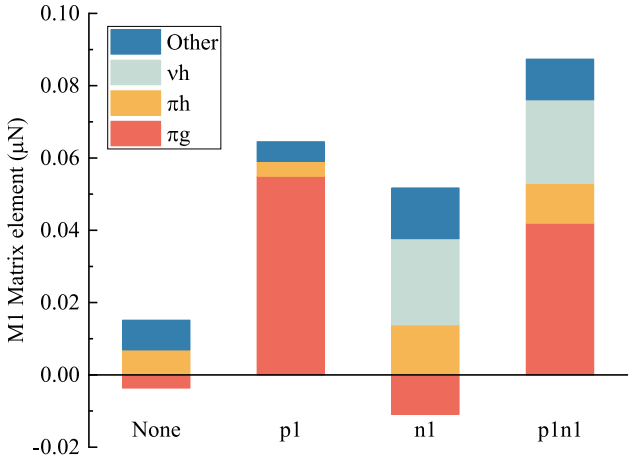

Fig. 3 (Color online) Decomposition of the M1 transition matrix elements calculated using the present Hamiltonian. Each matrix element is decomposed of the part involving the $\pi 0g_{7/2}$ and $\pi 0g_{9/2}$ orbitals (π g), that involving $\pi 0h_{11/2}$ (πh), that involving $\nu 0h_{9/2}$ and $\nu 0h_{11/2}$ (νh), and the others

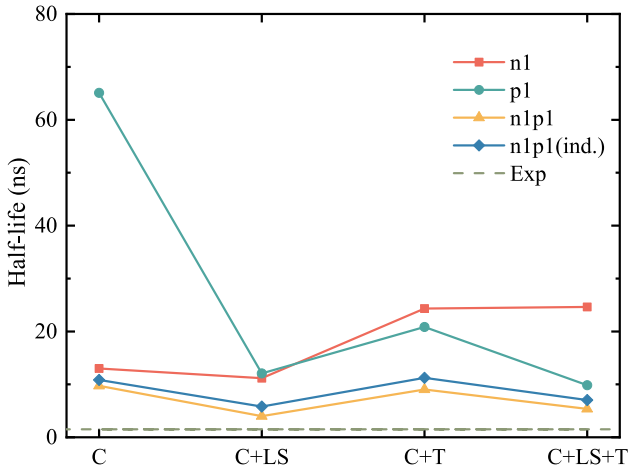

Fig. 4 (Color online) Comparison of half-lives of $5/2_1^+$ state in ^{139}La, derived with part of or all nuclear force components. "C," "LS," and "T" represent the central, spin-orbit, and tensor forces, respectively. "n1" and "p1" represent the inclusion of at most one neutron or proton core-excitation from the $\nu 0h_{11/2}$ and $\pi 0g_{9/2}$ orbitals, respectively. "n1p1(ind.)" is evaluated by considering "n1" and "p1" as independent branches. "n1p1" denotes the condition that both one neutron and proton core-excitations are allowed. For illustration, the experimental values are represented using dashed lines

core-excitation condition, all the corresponding components are available, whereas the major components originate from the spin-flip orbitals on both sides of the $Z = 50$ ($g_{7/2}$ and $g_{9/2}$) and $N = 82$ ($h_{11/2}$ and $h_{9/2}$) shells.

Herein, we aim to investigate the influence of the different components, including central, spin-orbit, and tensor parts, of effective interaction on the M1 transition strength, as shown in Fig. 4. The different nuclear-force components exhibited different behaviors with changes in the core-excitation truncation. In the p1 case, introducing the central force increases the half-life of the $5/2_1^+$ state in ^{139}La. Involving either tensor or spin-orbit forces significantly reduces the half-life, and an even lower value (as presented in Table 1) can be obtained by considering all forces. This finding is consistent with the experimental results. A different scenario is observed when only neutron core-excitation is involved in the shell model calculation (n1 case). Considering only the central force in the calculation significantly reduces the predicted half-life. Adding the spin-orbit or tensor force does not significantly change the result or even slightly increase the result when the tensor part is considered.

The significant difference between the p1 and n1 cases indicates that the tensor and spin-orbit forces contribute differently in both cases. This was unexpected because, as shown in Fig. 3, within the M1 matrix element, the πg component exhibits constructive and deconstructive interference with the other components in the p1 and n1 cases, respectively. Moreover, the νh component exists in the n1 case but not in the p1 condition, initiating a different situation when spin-orbital or tensor forces are generated. This observation is supported by the n1p1 case, in which the νh component is also a dominant contributor among the matrix elements, and the calculated half-life does not change significantly when spin-orbit and tensor forces are generated; a situation that is similar to the n1 case.

The n1p1(ind.) case, which is evaluated by considering n1 and p1 as independent branches, estimates an overall longer half-life than the "n1p1" condition. However, both cases exhibit similar tendencies. This implies that a consistent interference would be observed between the proton and neutron core-breaking components and that such an interference term between the proton and neutron configurations would not be sensitive to the nuclear force component. Changes in M1 transition strengths with respect to various nuclear forces reflect the modification of effective single-particle energies to adjust the configurations for both $5/2_1^+$ and $7/2_1^+$ in ^{139}La.

4 Conclusion

This study measured the lifetime of the first excited state in ^{139}La using a state-of-the-art $LaBr_3$ + plastic scintillator array in a digital data-acquisition system. Compared with previous measurements that used stilbene or plastic scintillators, the proposed measurement effectively separates the background contribution in the gamma line spectrum owing to the high energy resolution of $LaBr_3$. To measure the lifetime of the ($5/2_1^+$) state in ^{139}La, a comprehensive

shell-model study was conducted in a large model space. Results showed that both proton and neutron core-excitations were necessary to reproduce the measured lifetime of the $(5/2^+_1)$ state in ^{139}La. To reproduce the measured L-forbidden M1 transition strength, in addition to the core-excitation, a tensor correction was required for the effective M1 operator with a g-factor of 0.15, which is significantly smaller than the previously calculated value in this region or around ^{208}Pb.

Author Contributions All authors contributed to the study conception and design. Material preparation, data collection and analysis were performed by Zhi-Xuan Wang, Guang-Xin Zhang and Wei Jiang. The first draft of the manuscript was written by Zhi-Xuan Wang, and all authors commented on previous versions of the manuscript. All authors read and approved the final manuscript.

Data Availability The data that support the findings of this study are openly available in Science Data Bank at https://cstr.cn/31253.11.sciencedb.j00186.00678 and https://doi.org/10.57760/sciencedb.j00186.00678.

Declarations

Conflict of interest The authors declare that they have no conflict of interest.

References

1. I. Govil, C. Khurana, Systematics of l-forbidden M1 transitions. Nucl. Phys. **60**, 666–671 (1964). https://doi.org/10.1016/0029-5582(64)90102-6
2. A. Bohr, B.R. Mottelson, *Nuclear Structure Volume 1, page 336*, (World Scientific Publishing Company, 1998). https://doi.org/10.1142/3530
3. R. Bauer, J. Speth, V. Klemt et al., Magnetic multipole moments and transition probabilities of single-particle states around ^{208}Pb. Nucl. Phys. A **209**, 535–556 (1973). https://doi.org/10.1016/0375-9474(73)90845-2
4. C. Yuan, M. Liu, N. Shimizu et al., Shell-model study on spectroscopic properties in the region "south'' of ^{208}Pb. Phys. Rev. C **106**, 044314 (2022). https://doi.org/10.1103/PhysRevC.106.044314
5. T. Togashi, Y. Tsunoda, T. Otsuka et al., Novel shape evolution in sn isotopes from magic numbers 50 to 82. Phys. Rev. Lett. **121**, 062501 (2018). https://doi.org/10.1103/PhysRevLett.121.062501
6. G. Pasqualato, A. Gottardo, D. Mengoni et al., An alternative viewpoint on the nuclear structure towards ^{100}Sn: lifetime measurements in ^{105}Sn. Phys. Lett. B **845**, 138148 (2023). https://doi.org/10.1016/j.physletb.2023.138148
7. P.K. Joshi, B. Singh, S. Singh et al., Nuclear data sheets for A = 139. Nucl. Data Sheets **138**, 1–292 (2016). https://doi.org/10.1016/j.nds.2016.11.001
8. T. Gerholm, H. De Waard, The half-life of the 163 keV excited state in 139 Lanthanum. Physica **21**, 601–602 (1955). https://doi.org/10.1016/S0031-8914(55)90708-4
9. H. De Waard, T. Gerholm, Orbital momentum forbidden magnetic dipole transitions in some odd proton nuclei. Nucl. Phys. **1**, 281–301 (1956). https://doi.org/10.1016/0029-5582(56)90095-5
10. J. Geiger, R. Graham, I. Bergström et al., Measurements of M1 and E2 transition probabilities in Te^{125}, I^{127}, Xe^{129}, Cs^{133}, La^{139} and Pr^{141}. Nucl. Phys. **68**, 352–368 (1965). https://doi.org/10.1016/0029-5582(65)90652-8
11. J. Kownacki, J. Bialkowski, M. Moszynski et al., Adaptation of a long-lens beta-ray spectrometer for the measurement of short nuclear lifetimes. Nukleonika **15**, 649–59 (1970). https://api.semanticscholar.org/CorpusID:124486616
12. H. Cheng, B. Sun, L. Zhu et al., Intrinsic background radiation of $LaBr_3$(Ce) detector via coincidence measurements and simulations. Nucl. Sci. Tech. **31**, 99 (2020). https://doi.org/10.1007/s41365-020-00812-8
13. W. Lu, L. Wang, Y. Yuan et al., Monte carlo simulation for performance evaluation of detector model with a monolithic $LaBr_3$(Ce) crystal and sipm array for γ radiation imaging. Nucl. Sci. Tech. **33**, 107 (2022). https://doi.org/10.1007/s41365-022-01081-3
14. B. Bucher, H. Mach, A. Aprahamian et al., New lifetime measurements in ^{109}Pd and the onset of deformation at N=60. Phys. Rev. C **92**, 064312 (2015). https://doi.org/10.1103/PhysRevC.92.064312
15. H. Mach, R. Gill, M. Moszyński, A method for picosecond lifetime measurements for neutron-rich nuclei: (1) outline of the method. Nucl. Instrum. Methods A **280**, 49–72 (1989). https://doi.org/10.1016/0168-9002(89)91272-2
16. H. Jing, J. Tang, H. Tang et al., Studies of back-streaming white neutrons at CSNS. Nucl. Instrum. Methods A **621**, 91–96 (2010). https://doi.org/10.1016/j.nima.2010.06.097
17. B. Qi, Y. Li, D. Zhu et al., Measurement of the neutron beam profile of the back-n white neutron facility at CSNS with a micromegas detector. Nucl. Instrum. Methods A **957**, 163407 (2020). https://doi.org/10.1016/j.nima.2020.163407
18. J.Y. Tang, Q. An, J.B. Bai et al., Back-n white neutron source at CSNS and its applications. Nucl. Sci. Tech. **32**, 11 (2021). https://doi.org/10.1007/s41365-021-00846-6
19. J.M. Xue, S. Feng, Y.H. Chen et al., Measurement of the neutron-induced total cross sections of ^{nat}Pb from 0.3 ev to 20 MeV on the back-n at CSNS. Nucl. Sci. Tech. **35**, 18 (2024). https://doi.org/10.1007/s41365-024-01370-z
20. Q. Li, L.J. Wang, J.Y. Tang et al., ^{10} B-doped MCP detector developed for neutron resonance imaging at back-n white neutron source. Nucl. Sci. Tech. **35**, 142 (2024). https://doi.org/10.1007/s41365-024-01512-3
21. J.C. Wang, J. Ren, W. Jiang et al., In-beam gamma rays of CSNS back-n characterized by black resonance filter. Nucl. Sci. Tech. **35**, 164 (2024). https://doi.org/10.1007/s41365-024-01553-8
22. H. Chen, X.L. Wang, China's first pulsed neutron source. Nat. Mater. **15**, 689–691 (2016). https://doi.org/10.1038/nmat4655
23. H. Wu, Z. Li, H. Tan et al., A general-purpose digital data acquisition system (GDDAQ) at Peking university. Nucl. Instrum. Methods A **975**, 164200 (2020). https://doi.org/10.1016/j.nima.2020.164200
24. J. Chen, Nuclear data sheets for A=138. Nucl. Data Sheets **146**, 1–386 (2017). https://doi.org/10.1016/j.nds.2017.11.001
25. https://bricc.anu.edu.au/index.php
26. T. Otsuka, T. Suzuki, M. Honma et al., Novel features of nuclear forces and shell evolution in exotic nuclei. Phys. Rev. Lett. **104**, 012501 (2010). https://doi.org/10.1103/PhysRevLett.104.012501
27. G. Bertsch, J. Borysowicz, H. McManus et al., Interactions for inelastic scattering derived from realistic potentials. Nucl. Phys. A **284**, 399–419 (1977). https://doi.org/10.1016/0375-9474(77)90392-X
28. C. Yuan, T. Suzuki, T. Otsuka et al., Shell-model study of boron, carbon, nitrogen, and oxygen isotopes with a monopole-based universal interaction. Phys. Rev. C **85**, 064324 (2012). https://doi.org/10.1103/PhysRevC.85.064324
29. Y. Utsuno, T. Otsuka, B.A. Brown et al., Shape transitions in exotic Si and S isotopes and tensor-force-driven Jahn–Teller

effect. Phys. Rev. C **86**, 051301(R) (2012). https://doi.org/10.1103/PhysRevC.86.051301
30. T. Togashi, N. Shimizu, Y. Utsuno et al., Large-scale shell-model calculations for unnatural-parity high-spin states in neutron-rich Cr and Fe isotopes. Phys. Rev. C **91**, 024320 (2015). https://doi.org/10.1103/PhysRevC.91.024320
31. C. Yuan, Z. Liu, F. Xu et al., Isomerism in the "south-east'' of ^{132}Sn and a predicted neutron-decaying isomer in ^{129}Pd. Phys. Lett. B **762**, 237 (2016). https://doi.org/10.1016/j.physletb.2016.09.030
32. H.K. Wang, Z.H. Li, C.X. Yuan et al., Monopole effects, core excitations, and β decay in the A= 130 hole nuclei near ^{132}Sn. Chin. Phys. C **43**, 054101 (2019). https://doi.org/10.1088/1674-1137/43/5/054101
33. Z.Y. Zhang, H.B. Yang, M.H. Huang et al., New alpha-emitting isotope ^{214}U and abnormal enhancement of alpha-particle clustering in lightest uranium isotopes. Phys. Rev. Lett. **126**, 152502 (2021). https://doi.org/10.1103/PhysRevLett.126.152502
34. H.B. Yang, Z.G. Gan, Z.Y. Zhang et al., New isotope Th^{207} and odd-even staggering in α -decay energies for nuclei with $Z > 82$ and $N < 126$. Phys. Rev. C **105**, L051302 (2022). https://doi.org/10.1103/PhysRevC.105.L051302
35. W. Hua, Z. Zhang, L. Ma et al., Fine structure of α decay in ^{222}Pa. Chin. Phys. C **45**, 044001 (2021). https://doi.org/10.1088/1674-1137/abdea8
36. C.X. Yuan, Y.L. Ge, M.L. Liu et al., Recent shell-model investigation and its possible role in nuclear structure data study. EPJ Web Conf. **239**, 04002 (2020). https://doi.org/10.1051/epjconf/202023904002
37. M. Liu, C. Yuan, Recent progress in configuration-interaction shell model. Int. J Mod. Phys. E **23**, 2330003 (2023). https://doi.org/10.1142/S0218301323300035
38. J. Chen, M. Liu, C. Yuan et al., Shell-model-based investigation on level density of Xe and Ba isotopes. Phys. Rev. C **107**, 054306 (2023). https://doi.org/10.1103/PhysRevC.107.054306
39. N. Shimizu, arXiv: 1310.5431 (2013)
40. I. Towner, Quenching of spin matrix elements in nuclei. Phys. Rep. **155**, 263–377 (1987). https://doi.org/10.1016/0370-1573(87)90138-4
41. G. White, N. Stone, J. Rikovska et al., Magnetic dipole moments near ^{132}Sn: new measurement on ^{135}I by NMR/ON. Nucl. Phys. A **644**, 277–288 (1998). https://doi.org/10.1016/S0375-9474(98)00597-1
42. B.A. Brown, N.J. Stone, J.R. Stone et al., Magnetic moments of the 2_1^+ states around ^{132}Sn. Phys. Rev. C **71**, 044317 (2005). https://doi.org/10.1103/PhysRevC.71.044317
43. Mesons in Nuclei, p.718., (North-Holland Publishing Company, Eds. M. Rho and D. H. Wilkinson), (1979)
44. W. Andrejtscheff, L. Zamick, N. Marupov et al., Core polarization for l-forbidden M1 transitions in light nuclei. Nucl. Phys. A **351**, 54–62 (1981). https://doi.org/10.1016/0375-9474(81)90544-3